Analysis of Narrowband Communication Systems Impaired by MB-OFDM UWB Interference

Journal:	*IEEE Transactions on Wireless Communications*
Manuscript ID:	Paper-TW-Apr-06-0203.R1
Manuscript Type:	Original Transactions Paper
Date Submitted by the Author:	09-Sep-2006
Complete List of Authors:	Nasri, Amir; University of British Columbia, Electrical and Computer Engineering Schober, Robert; University of British Columbia, Electrica and Computer Engineering Lampe, Lutz; University of British Columbia, Electrical and Computer Engineering
Keyword:	UWB < Transmission Technology, Detection and Estimation < Transmission Technology

Analysis of Narrowband Communication Systems Impaired by MB–OFDM UWB Interference[1]

Amir Nasri, Robert Schober, and Lutz Lampe

Department of Electrical and Computer Engineering

The University of British Columbia

2356 Main Mall, Vancouver, BC, V6T 1Z4, Canada

Phone: +604 - 822 - 3515

Fax: +604 - 822 - 5949

E-mail: {amirn, rschober, lampe}@ece.ubc.ca

Abstract

In this paper, we investigate the effect of multi–band orthogonal frequency division multiplexing (MB–OFDM) ultra–wideband (UWB) interference on narrowband (NB) receivers. For this purpose, we first derive the exact moment generating function of MB–OFDM UWB interference. Based on this result, we develop analytical expressions for the amplitude probability distribution (APD) and the bit error rate (BER) of a binary phase–shift keying NB receiver. These expressions can be efficiently numerically evaluated and the presented analysis is general enough to encompass non–fading and various fading NB channels. We show that for NB signals with, respectively, much smaller and much larger bandwidths than the MB–OFDM sub–carrier spacing a Gaussian approximation (GA) and an impulsive GA (IGA) of the MB–OFDM UWB interference lead to accurate performance predictions. However, for most NB channel models and signal bandwidths the exact BER analysis has to be used to obtain meaningful results. An exception is the Rayleigh fading NB channel where both GA and IGA yield tight approximations of the exact BER regardless of the NB signal bandwidth.

[1]This work was presented in part at the IEEE Vehicular Technology Conference (Spring–VTC), Melbourne, May 2006, and in part at the IEEE International Conference on Communications (ICC), Istanbul, June 2006.

1 Introduction

In 2002, the US Federal Communications Commission (FCC) opened the frequency range from 3.1 GHz to 10.6 GHz for unlicensed operation of ultra–wideband (UWB) radios with a maximum power spectral density of -41.3 dBm/MHz. Since then UWB has emerged as an important technology for short–range high data rate wireless communication. A natural consequence of the unprecedented large bandwidth of UWB signals is the potential of causing harmful interference to narrowband (NB) systems. Although ideally UWB interference should be negligible compared to the Gaussian background noise, depending on the location of the UWB interferer this may not be true considering a thermal noise floor of -114 dBm/MHz. Therefore, it is important to accurately investigate the performance degradation of coexisting NB receivers in the presence of UWB interference.

Most existing UWB interference studies have considered either direct–sequence UWB (DS–UWB) or impulse radio time–hopping UWB (TH–UWB), cf. e.g. [1, 2, 3, 4]. The literature on multi–band orthogonal frequency division multiplexing (MB–OFDM) UWB interference is comparatively sparse. This is surprising as MB–OFDM UWB had been a strong candidate for standardization by the IEEE for high–rate wireless personal area networks (WPANs) [5] and has been recently adopted as a standard by the ECMA [6]. In [7, 8], it has been shown that the interference from MB–OFDM UWB devices can be modeled as impulsive noise if the bandwidth of the victim receiver contains several MB–OFDM sub–carriers. The impact of MB–OFDM interference on an IEEE 802.11a wireless local area network (WLAN) receiver was evaluated experimentally in [9], while the impact of MB–OFDM interference on a C–band digital television (DTV) receiver was studied via simulations and experiments in [10] and [11], respectively. However, a general and exact analysis of MB–OFDM UWB interference is not available in the literature, and the impact of MB–OFDM UWB on the performance of NB receivers is not well understood.

In this paper, we provide a comprehensive analysis of MB–OFDM UWB interference and make the following contributions.

- We derive the exact moment generating function (MGF) and the exact amplitude probability distribution (APD) [11] of MB–OFDM UWB interference.
- Based on the MGF, we derive analytical expressions for the exact bit error rate (BER) of a binary phase–shift keying (BPSK) NB receiver impaired by MB–OFDM UWB interference and additive white Gaussian noise (AWGN). The obtained expressions allow for an efficient numerical evaluation and are applicable to non–fading channels as well as all commonly encountered

fading channel models including Rayleigh, Ricean, Nakagami–m, and Nakagami–q fading.

- For NB signal bandwidths much smaller and much larger than the MB–OFDM sub–carrier spacing, we show that the MB–OFDM interference model can be simplified using a Gaussian approximation (GA) and an impulsive GA (IGA), respectively. We provide the MGF for the GA and the IGA, respectively, and derive the corresponding APD and BER expressions for BPSK NB receivers.
- Exploiting the obtained APD and BER results we show that the accuracy of the GA and the IGA does not only depend on the NB signal bandwidth but also on the properties of the NB channel. We demonstrate that for Rayleigh fading and sufficiently high signal–to–interference ratios the BERs for GA and IGA are identical and closely approximate the exact BER regardless of the NB signal bandwidth. For other fading models and non–fading channels GA and IGA generally become accurate if $B_s < 0.05\Delta f$ and $B_s > 5\Delta f$, respectively, where B_s and Δf denote the NB signal bandwidth and the MB–OFDM sub–carrier spacing, respectively.
- For $0.05\Delta f \leq B_s \leq 5\Delta f$ the provided exact BER expressions have to be used to obtain meaningful results. For these NB signal bandwidths the BER of the NB receiver strongly depends on the carrier frequency offset between NB signal and MB–OFDM signal, the NB signal bandwidth, the number of MB–OFDM frequency bands, and the NB pulse shape.

Organization: In Section 2, the considered system and transmission model is introduced. In Section 3, the exact MGF of MB–OFDM UWB interference and two simple approximations thereof are derived, and exact and approximate expressions for the APD of MB–OFDM are provided. Exact and approximate BER expressions for a BPSK NB receiver impaired by MB–OFDM UWB interference, AWGN, and (possibly) fading are developed in Section 4. Numerical results are presented and discussed in Section 5, and conclusions are drawn in Section 6.

Notation: In this paper, $[\cdot]^*$, $\mathcal{E}\{\cdot\}$, $\Pr\{A\}$, and $\otimes$ denote complex conjugation, statistical expectation, the probability of event A, and convolution, respectively. In addition, $\Re\{\cdot\}$ and $\Im\{\cdot\}$ refer to the real and imaginary parts of a complex number, respectively.

2 System Model

In this section, the considered signal and channel model is introduced. In addition, the MB–OFDM UWB signal and the NB receiver processing are described in detail.

2.1 Signal and Channel Model

We consider the scenario where an MB–OFDM UWB transmitter is in close proximity to a coherent NB receiver. In order to capture the main effects of MB–OFDM interference on an NB signal while maintaining mathematical tractability, we adopt the same simple channel model[2] as e.g. [2, 9, 8]. In particular, the received signal in equivalent complex baseband representation is modeled as

$$r(t) = a_c(t)\, s(t) + g\, e^{j\theta_g}\, i(t-\tau) + n(t), \tag{1}$$

where $s(t)$, $i(t)$, and $n(t)$ denote the transmitted NB signal, the transmitted MB–OFDM UWB (interference) signal, and AWGN with one–sided power spectral density N_0, respectively. We assume that the NB channel is approximately time invariant during one NB symbol duration T_s. Therefore, the NB channel gain can be modeled as a constant $a_c(t) = a_c \triangleq a\, e^{j\theta_a}$, where $a \triangleq |a_c|$ and θ_a denote the magnitude and the phase of a_c, respectively. For non–fading channels $a = 1$, whereas for fading channels a is a positive random variable with probability density function (pdf) $p_a(a)$ and variance $\sigma_a^2 \triangleq \mathcal{E}\{a^2\} = 1$. Due to the proximity of the MB–OFDM transmitter and the NB receiver and the lack of synchronization between the two devices, the associated channel is modeled as non–fading with constant magnitude g and uniformly distributed phase $\theta_g \in [-\pi, \pi)$. The relative delay τ of the MB–OFDM signal compared to the NB signal is uniformly distributed in the interval $[0, T_s)$.

The NB signal $s(t)$ is given by

$$s(t) = \sqrt{\frac{E_s}{T_s}} \sum_{k=-\infty}^{\infty} b[k]\, p(t - kT_s), \tag{2}$$

where E_s, $b[k]$, and $p(t)$ denote the symbol energy, the kth transmit symbol, and the NB pulse shape, respectively. Although our analysis can be extended to any quadrature amplitude modulation (QAM) and pulse amplitude modulation (PAM) format using the general approach[3] presented in [15], we assume in the following BPSK modulation, i.e., $b[k] \in \{\pm 1\}$. This simplifies the exposition but all fundamental and qualitative results obtained in this paper also apply to higher order modulations.

[2]We note that for large NB signal bandwidths a more elaborate, frequency–selective channel model may be more appropriate. However, for such a model an analytical interference study may not be feasible. In addition, our results in Fig. 8 suggest that frequency selectivity of the interference channel does not have a large impact on the error rate of the NB system.

[3]In [15], it has been shown that the BER of PAM can be expressed as a sum of terms $w_i P_e(b_i a)$ where w_i and b_i are constellation dependent constants and $P_e(a)$ is the BER for BPSK for channel amplitude a. A similar statement is true for the QAM case, cf. [15].

Furthermore, we assume that $p(t)$ has a square–root Nyquist (SRN) frequency response [12], which is true for example for band–limited square–root raised cosine (SRRC) and time–limited rectangular (REC) pulse shapes.

2.2 MB–OFDM UWB Signal Model

The adopted model for the MB–OFDM UWB transmit signal $i(t)$ closely follows the IEEE.802.15.3a standard proposal [5]. More precisely, $i(t)$ is modeled as [5]

$$i(t) = \frac{1}{\sqrt{N_s}} \left(\sum_{k=-\infty}^{\infty} \sum_{\substack{n=-N_s/2 \\ n\neq 0}}^{N_s/2} a_n[k]\, e^{j2\pi n \Delta f (t-kT_i)}\, w(t-kT_i)\, \mathrm{e}^{j2\pi f_{\mathrm{MB}}[k] t} \right) \mathrm{e}^{j2\pi f_0 t}, \tag{3}$$

where N_s, Δf, and T_i denote the number of non–null sub–carriers, the sub–carrier spacing, and the OFDM symbol duration, respectively, and where we took into account that the zeroth sub–carrier is a null sub–carrier. In the following, we discuss the remaining variables in Eq. (3) more in detail.

MB–OFDM data symbols $a_n[k]$*:* The MB–OFDM data symbols $a_n[k]$ are taken from a 4–QAM alphabet, i.e., $a_n[k] \in \{\pm 1 \pm j\}$, and their statistical properties influence the interference statistics. The standard proposal [5] specifies seven different data rate modes. All modes involve channel coding but this does not have a noticeable effect on the interference statistics since the coded bits are interleaved before they are mapped to $a_n[k]$. Therefore, for MB–OFDM data rates of 320 and 480 Mb/s the data symbols $a_n[k]$ can be assumed independent, identically distributed (i.i.d.) with respect to both time index k and sub–carrier index n. In contrast, for data rates below 320 Mb/s each OFDM symbol is repeated once in time, i.e., $a_n[2k] = a_n[2k+1]$, $\forall k$, and for the two lowest data rates (55 and 80 Mb/s) the MB–OFDM data symbols have also a conjugate symmetry with respect to sub–carrier index n, i.e., $a_n[k] = a^*_{-n}[k]$, $1 \leq n \leq N_s/2$.

OFDM pulse shape $w(t)$*:* The OFDM pulse shape $w(t)$ is rectangular and given by [5]

$$w(t) = \begin{cases} 1 & T_P \leq t < T_i - T_G \\ 0 & \text{otherwise} \end{cases} \tag{4}$$

where T_P and $T_G \triangleq T_i - (T_P + 1/\Delta f)$ denote the prefix duration and the guard interval, respectively.

Frequency offsets f_0 *and* $f_{\mathrm{MB}}[k]$*:* $f_{\mathrm{MB}}[k]$ and f_0 are a time–dependent, periodic and a constant frequency offset, respectively. $f_{\mathrm{MB}}[k] \in \{(n_b - 1) N_s \Delta f \,|\, n_b \in \{1, 2, \ldots, N_B\}\}$ is used to switch between the N_B MB–OFDM frequency bands [5], and f_0 represents the offset of the NB signal with

respect to the zeroth sub–carrier of the first MB–OFDM band ($f_{\mathrm{MB}}[k] = 0$). Each MB–OFDM frequency band is active only $100/N_B$ % of the time, and the order in which the different bands are used is determined by a so–called time–frequency code. In the following, we assume that the time–frequency code

$$f_{\mathrm{MB}}[k] = (k \bmod N_B) N_s \Delta f, \tag{5}$$

is applied and that the NB signal lies fully in the first MB–OFDM frequency band. We note that our analysis can be easily adapted to the case where the NB signal is affected by two MB–OFDM frequency bands and to other time–frequency codes. In general, different time–frequency codes will lead to different NB system error rates. The frequency hopping of the MB–OFDM signal and its effect on the NB signal are schematically shown in frequency and time domain in Figs. 1a) and 1b), respectively. In Fig. 1, $N_B = 3$ is valid and for the time domain representation of the MB–OFDM signal only the contribution of the relevant first frequency band is depicted.

For all numerical examples presented in Section 5 the MB–OFDM parameters are chosen according to standard proposal [5] unless stated otherwise, cf. Table 1.

2.3 NB Receiver Processing

The NB receiver performs matched filtering and sampling of the continuous–time received signal $r(t)$. Taking into account the SRN property of the NB pulse shape $p(t)$ and the normalization $\int_{-\infty}^{\infty} |p(t)|^2 \, \mathrm{d}t = \sqrt{T_s/E_s}$, the discrete–time received signal can be expressed as

$$r_c[k] = r(t) \otimes p^*(-t)|_{t=kT_s} = a_c \, b[k] + i_c[k] + n_c[k], \tag{6}$$

where $i_c[k] \triangleq g \, e^{j\theta_g} \, i(t-\tau) \otimes p^*(-t)|_{t=kT_s}$ and $n_c[k]$ denote the complex MB–OFDM UWB interference and the complex AWGN, respectively. The resulting decision variable for BPSK transmission is

$$r[k] \triangleq \Re\{e^{-j\theta_a} r_c[k]\} = a \, b[k] + i[k] + n[k], \tag{7}$$

with real AWGN $n[k] \triangleq \Re\{e^{-j\theta_a} n_c[k]\}$ and

$$i[k] \triangleq \Re\{e^{-j\theta_a} i_c[k]\} = \Re\{g \, e^{j\theta} \, i(t-\tau) \otimes p^*(-t)|_{t=kT_s}\}, \tag{8}$$

where phase $\theta \triangleq \theta_g - \theta_a$ is uniformly distributed in $[-\pi, \pi)$. The estimated data symbol $\hat{b}[k]$ is obtained as $\hat{b}[k] = 1$ if $r[k] \geq 0$ and $\hat{b}[k] = -1$ if $r[k] < 0$.

For future reference, we define the signal–to–noise ratio (SNR) and the signal–to–interference ratio (SIR) as

$$\mathrm{SNR} \triangleq \frac{\mathcal{E}\{(ab[k])^2\}}{\mathcal{E}\{2(n[k])^2\}} = \frac{1}{2\sigma_n^2} = \frac{E_s}{N_0} \qquad \text{and} \qquad \mathrm{SIR} \triangleq \frac{\mathcal{E}\{(ab[k])^2\}}{\mathcal{E}\{2(i[k])^2\}} = \frac{1}{2\sigma_i^2}, \tag{9}$$

respectively. Here, $\sigma_n^2 \triangleq \mathcal{E}\{(n[k])^2\}$ and $\sigma_i^2 \triangleq \mathcal{E}\{(i[k])^2\}$ denote the variance of $n[k]$ and the variance of $i[k]$, respectively.

3 MB–OFDM UWB Interference Analysis

In this section, we first derive an expression for the exact MGF $\Phi_{i,\mathrm{E}}(s)$ of the MB–OFDM UWB interference $i[k]$. Subsequently two approximate models for MB–OFDM UWB interference are provided and the associated MGFs are given. In addition, exact and approximate expressions for the APD are developed.

3.1 Exact Moment Generating Function (MGF) of $i[k]$

Before we calculate the exact MGF, we first reformulate and simplify the analytical expression for $i[k]$.

3.1.1 Reformulation of $i[k]$

Based on Eqs. (3) and (8) the MB–OFDM interference signal can be expressed as

$$i[k] = \Re\left\{ \sum_{\kappa=-\infty}^{\infty} \sum_{\substack{n=-N_s/2 \\ n\neq 0}}^{N_s/2} g\, e^{j\theta}\, \alpha_n(kT_s - \kappa T_i - \tau)\, a_n[\kappa] \right\}, \tag{10}$$

where the coefficients $\alpha_n(kT_s - \kappa T_i - \tau)$ are defined as

$$\alpha_n(kT_s - \kappa T_i - \tau) \triangleq \frac{1}{\sqrt{N_s}} p^*(-t) \otimes e^{j2\pi n \Delta f (t-\tau-\kappa T_i)} w(t - \tau - \kappa T_i)\, e^{j2\pi (f_{\mathrm{MB}}[\kappa] + f_0)(t-\tau)} \Big|_{t=kT_s}. \tag{11}$$

Adopting the time–frequency code in Eq. (5) and assuming that the NB signal lies fully in the first MB–OFDM frequency band, Eq. (10) can be simplified to

$$i[k] = \Re\left\{ \sum_{\kappa=-\infty}^{\infty} \sum_{\substack{n=-N_s/2 \\ n\neq 0}}^{N_s/2} g\, e^{j\theta}\; e^{j2\pi f_0 N_B \kappa T_i}\, \beta_n(\tau_k - N_B \kappa T_i)\, a_n[N_B \kappa] \right\}, \tag{12}$$

where $\tau_k \triangleq kT_s - \tau$ and $\beta_n(t)$ is given by

$$\beta_n(t) = \frac{1}{\sqrt{N_s}} \int_{-\infty}^{\infty} e^{j2\pi(n\Delta f + f_0)u}\, p^*(u-t)\, w(u)\, \mathrm{d}u = \frac{1}{\sqrt{N_s}} \int_{T_P}^{T_i - T_G} e^{j2\pi(n\Delta f + f_0)u} p^*(u-t)\, \mathrm{d}u. \quad (13)$$

Alternatively, using Parseval's theorem [12], $\beta_n(t)$ may be obtained from

$$\beta_n(t) = e^{j2\pi(n\Delta f + f_0)t} \frac{1}{\sqrt{N_s}} \int_{-\infty}^{\infty} e^{j2\pi f(t - [1/(2\Delta f) + T_P])} P^*(f + n\Delta f + f_0)\, \frac{\sin(\pi f/\Delta f)}{\pi f}\, \mathrm{d}f, \quad (14)$$

where $P(f)$ denotes the Fourier transform of $p(t)$. Since any NB pulse shape $p(t)$ is essentially limited in time and frequency, the coefficients $\beta_n(\tau_k - N_B \kappa T_i)$ are approximately zero if, respectively, κ and n exceed certain upper and lower limits, cf. Eqs. (13) and (14).

We note that for other time–frequency codes specified in [5] similar simplified expressions for $i[k]$ can be found.

3.1.2 Conditional Moment Generating Function

Now, we are ready to derive the MGF of $i[k]$ conditioned on τ_k and phase offset θ[4]

$$\Phi_{i|\theta,\tau_k}(s) \triangleq \mathcal{E}\{e^{-s\, i[k]} | \theta, \tau_k\}. \quad (15)$$

For evaluation of Eq. (15), the statistical properties of the MB–OFDM data symbols $a_n[k]$ are important. We first note that because of the frequency hopping dictated by the time–frequency code in Eq. (5) the NB signal is affected only by every N_Bth MB–OFDM symbol. Therefore, assuming $N_B \geq 2$ the repetition of every MB–OFDM symbol in time for data rates below 320 Mb/s has no impact on the interference statistics. However, the dependence introduced by the conjugate symmetry for MB–OFDM data rates of 55 and 80 Mb/s affects the interference statistics seen by the NB signal if the NB signal spectrum is non–zero for both positive and negative sub–carrier frequencies. Therefore, we consider in the following two different cases.

C1) No conjugate symmetry (MB–OFDM data rates of more than 80 Mb/s): In this case, the MB–OFDM data symbols can be modeled as i.i.d. random variables and using Eq. (12) we can

[4]Although Eq. (15) differs from the usual definition of the MGF by the negative sign in the exponential, we still refer to $\Phi_{i|\theta,\tau_k}(s)$ as MGF. Strictly speaking $\Phi_{i|\theta,\tau_k}(s)$ as defined in Eq. (15) is the *Laplace transform* of the conditional pdf of $i[k]$.

rewrite Eq. (15) as

$$\Phi_{i|\theta,\tau_k}(s) = \prod_{\kappa=-\infty}^{\infty} \prod_{\substack{n=-N_s/2 \\ n\neq 0}}^{N_s/2} \mathcal{E}\left\{\exp\left(-s\Re\left\{g e^{j\theta} e^{j2\pi f_0 N_B \kappa T_i} \beta_n(\tau_k - N_B\kappa T_i) a_n[N_B\kappa]\right\}\right) \middle| \theta, \tau_k\right\}. \quad (16)$$

If we furthermore take into account that the MB–OFDM data symbols are equi–probable 4–QAM symbols, we arrive at the conditional MGF

$$\begin{aligned}\Phi_{i|\theta,\tau_k}(s) &= \prod_{\kappa=-\infty}^{\infty} \prod_{\substack{n=-N_s/2 \\ n\neq 0}}^{N_s/2} \cosh\left(s\,\Re\{g e^{j\theta} e^{j2\pi f_0 N_B \kappa T_i} \beta_n(\tau_k - N_B\kappa T_i)\}\right) \\ &\qquad \cosh\left(s\,\Im\{g e^{j\theta} e^{j2\pi f_0 N_B \kappa T_i} \beta_n(\tau_k - N_B\kappa T_i)\}\right). \quad (17)\end{aligned}$$

Finally, for numerical evaluation of $\Phi_{i|\tau_k,\theta}(s)$ we replace Eq. (17) by

$$\begin{aligned}\Phi_{i|\theta,\tau_k}(s) &\simeq \prod_{\kappa=-\kappa_l}^{\kappa_u} \prod_{\substack{n=-n_l \\ n\neq 0}}^{n_u} \cosh\left(s\,\Re\{g e^{j\theta} e^{j2\pi f_0 N_B \kappa T_i} \beta_n(\tau_k - N_B\kappa T_i)\}\right) \\ &\qquad \cosh\left(s\,\Im\{g e^{j\theta} e^{j2\pi f_0 N_B \kappa T_i} \beta_n(\tau_k - N_B\kappa T_i)\}\right), \quad (18)\end{aligned}$$

where κ_l, κ_u, n_l, and n_u are suitably chosen upper and lower limits which ensure $\beta_n(\tau_k - N_B\kappa T_i)\} \approx 0$ if $\kappa \notin [-\kappa_l,\, \kappa_u]$ or $n \notin [-n_l,\, n_u]$, cf. Section 3.1.1. Depending on the system parameters, typically 20 to 100 terms are required in Eq. (18) to achieve an accurate approximation of Eq. (17).

C2) Conjugate symmetry (MB–OFDM data rates of 55 and 88 Mb/s): Using similar steps as above but taking into account $a_n[k] = a^*_{-n}[k]$, $1 \le n \le N_s/2$, the conditional MGF is obtained as

$$\begin{aligned}\Phi_{i|\theta,\tau_k}(s) &= \prod_{\kappa=-\infty}^{\infty} \prod_{n=1}^{N_s/2} \cosh\left(s\,\Re\{g e^{j\theta} e^{j2\pi f_0 N_B \kappa T_i} \gamma_n(\tau_k - N_B\kappa T_i)\}\right) \\ &\qquad \cosh\left(s\,\Im\{g e^{j\theta} e^{j2\pi f_0 N_B \kappa T_i} \delta_n(\tau_k - N_B\kappa T_i)\}\right), \quad (19)\end{aligned}$$

where $\gamma_n(t) \triangleq \beta_n(t) + \beta_{-n}(t)$ and $\delta_n(t) \triangleq \beta_n(t) - \beta_{-n}(t)$. For numerical evaluation of Eq. (19) the products can be truncated in a similar way as in Eq. (18).

In the remainder of this paper, we will assume Case C1) and i.i.d. MB–OFDM data symbols. However, all analytical results presented are also valid for Case C2) and conjugate symmetric data symbols if the conditional MGF in Eq. (19) is used instead of the one in Eq. (17).

3.1.3 Exact Moment Generating Function

Since we assume that both the phase offset θ_g and the delay τ of the MB–OFDM interferer are uniformly distributed random variables, cf. Section 2.1, we have to average $\Phi_{i|\theta,\tau_k}(s)$ with respect

to θ_g and τ or equivalently with respect to θ and τ_k, respectively. After averaging over θ, we can express the MGF of $i[k]$ conditioned τ_k as

$$\Phi_{i|\tau_k}(s,\,\tau_k) \triangleq \mathcal{E}\{\Phi_{i|\theta,\tau_k}(s)\} = \frac{1}{2\pi}\int_{2\pi}\Phi_{i|\theta,\tau_k}(s)\,\mathrm{d}\theta. \tag{20}$$

Since it is shown in Appendix A that $\Phi_{i|\tau_k}(s,\,\tau_k)$ is periodic in τ_k with period N_BT_i, the unconditional MGF can be obtained by averaging $\Phi_{i|\tau_k}(s,\,\tau_k)$ over any interval of length N_BT_i. Since τ is assumed to be uniformly distributed, τ_k is also uniformly distributed and the exact MGF of $i[k]$ can be computed as

$$\Phi_{i,\,\mathrm{E}}(s) = \frac{1}{2\pi N_BT_i}\int_{N_BT_i}\int_{2\pi}\Phi_{i|\theta,\tau_k}(s)\,\mathrm{d}\theta\,\mathrm{d}\tau_k. \tag{21}$$

$\Phi_{i,\,\mathrm{E}}(s)$ can be efficiently numerically evaluated as Eq. (21) only involves two integrals with finite limits and $\Phi_{i|\theta,\tau}(s)$ may be replaced by the approximation in Eq. (18).

3.2 Approximate Models for MB–OFDM UWB Interference

In this subsection, we discuss two simplified MB–OFDM UWB interference models which are good approximations of the exact model if the NB signal bandwidth $B_s \triangleq 1/T_s$ is much smaller and much larger than the MB–OFDM sub–carrier spacing Δf, respectively.[5]

3.2.1 Gaussian Approximation (GA)

We first consider the case where the NB signal has a very small bandwidth B_s compared to the sub–carrier spacing frequency Δf, i.e., $B_s \ll \Delta f$ which also implies $T_s \gg T_i$. In this case, Eqs. (13) and (14) show, respectively, that $\beta_n(\tau_k - N_B\kappa)$ is non–zero over a large interval of κ and a small interval of n since $p(t)$ is a broad pulse in the time domain whereas $P(f)$ is a narrow pulse in the frequency domain. Therefore, in Eq. (12) for certain values of n many independent random variables with non–zero (and similar) variances are added in the summation over κ. This suggests that the central limit theorem can be invoked and $i[k]$ may be approximated as a real Gaussian random variable with MGF

$$\Phi_{i,\,\mathrm{GA}}(s) = e^{s^2\sigma_i^2/2}. \tag{22}$$

[5]We note that the exact amount of spectrum occupied by the NB signal heavily depends on the adopted pulse shape $p(t)$, of course. In order to facilitate a unified treatment of different pulse shapes, we refer to $B_s = 1/T_s$ as the NB signal bandwidth here.

In this case, the multi–band nature of the MB–OFDM UWB interference does not affect the MGF. We note however that for a given B_s the number of non–zero terms added in Eq. (12) decreases with increasing N_B implying that the GA becomes less accurate.

3.2.2 Impulsive Gaussian Approximation (IGA)

Now, we assume that the bandwidth B_s of the NB signal[6] is large compared to the sub–carrier spacing frequency Δf, i.e., $B_s \gg \Delta f$ and $T_s \ll T_i$. Thus, if $f_{\mathrm{MB}}[k] = 0$ the MB–OFDM signal impairs the NB signal for several NB symbol durations T_s. After the MB–OFDM signal has hopped to a different center frequency $f_{\mathrm{MB}}[k] > 0$ it will not affect the NB signal for a duration of $N_B T_i - 1/\Delta f$, where we took into account that $i[k]$ is also zero during the prefix and the guard interval. These time–domain considerations show that only approximately a fraction of $\rho \triangleq 1/(N_B \Delta f T_i)$ NB symbols are affected by the MB–OFDM signal.

If an NB symbol is impaired by the MB–OFDM signal (i.e., if $f_{\mathrm{MB}}[k] = 0$), $\beta_n(\tau_k - N_B\kappa)$ will have non–zero values only for a single value of $\kappa = \kappa_0$. However, for κ_0, $\beta_n(\tau_k - N_B\kappa_0)$ will be non–zero for a large number of sub–carriers n since $P(f)$ is a broad pulse, cf. Eq. (14). Therefore, $i[k]$ in Eq. (12) involves a sum of many independent random variables with similar variances and the central limit theorem applies.

To summarize, for $B_s \gg \Delta f$, $100\,\rho$ % of the NB symbols are impaired by approximately Gaussian interference, whereas $100\,(1-\rho)$ % of the NB symbols do not experience any interference. Therefore, in this case, the MGF of $i[k]$ can be approximated as

$$\Phi_{i,\,\mathrm{IGA}}(s) = 1 - \rho + \rho\, e^{s^2\sigma_i^2/(2\rho)}. \tag{23}$$

We note that similar IGA models for MB–OFDM have also been reported in [7, 8].

3.3 Amplitude Probability Distribution (APD)

The National Telecommunications and Information Administration (NTIA) recommends APDs for assessment of UWB waveforms [7, 11]. The APD is the complementary cumulative distribution function of the amplitude of the interference signal $i[k]$

$$\mathrm{APD}(y) \triangleq \Pr\{|i[k]| > y\}. \tag{24}$$

[6]Here, "narrowband" means that the bandwidth of the signal is small compared to the total MB–OFDM UWB bandwidth, i.e., $B_s \ll N_B N_s \Delta f$.

We note that the APD as defined in Eq. (24) deviates slightly from the one in [7, 11]. In [7, 11] the APD of the complex UWB interference $i_c[k]$ is considered, whereas we consider the APD of the real interference $i[k]$, cf. Eq. (8), since only $i[k]$ affects the decision variable, cf. Eq. (7). For the GA and the IGA it is straightforward to show that the corresponding APDs are given by

$$\mathrm{APD}_{\mathrm{GA}}(y) = 2\,Q\left(\sqrt{\frac{y^2}{\sigma_i^2}}\right) \tag{25}$$

and

$$\mathrm{APD}_{\mathrm{IGA}}(y) = 2\rho\,Q\left(\sqrt{\frac{\rho y^2}{\sigma_i^2}}\right), \tag{26}$$

respectively, where $Q(x) \triangleq \frac{1}{\sqrt{2\pi}}\int_x^\infty e^{-t^2/2}\,\mathrm{d}t$ denotes the Gaussian Q–function [12]. For the exact MB–OFDM interference model a closed–form expression for the APD cannot be found but $\mathrm{APD}_{\mathrm{E}}(y)$ can be evaluated numerically. For this purpose it is useful to note that the exact pdf $p_{i,\,\mathrm{E}}(x)$ of $i[k]$ is an even function of x, since its Fourier transform $\Phi_{i,\,\mathrm{E}}(j\omega)$ is a real and even function of ω [13]. Therefore, exploiting basic properties of the Laplace transform [14], we can express the exact APD as

$$\mathrm{APD}_{\mathrm{E}}(y) = 2\int_{-\infty}^{-y} p_{i,\,\mathrm{E}}(x)\,\mathrm{d}x = \frac{1}{\pi j}\int_{c-j\infty}^{c+j\infty} \Phi_{i,\,\mathrm{E}}(s)\,e^{-ys}\,\frac{\mathrm{d}\,s}{s}, \tag{27}$$

where c is a positive constant lying in the region of convergence of the integral. An efficient numerical evaluation of Eq. (27) is possible by applying a Gauss–Chebyshev quadrature rule, cf. e.g. [14]. This results in

$$\mathrm{APD}_{\mathrm{E}}(y) \simeq \frac{2}{K}\sum_{k=1}^{K/2}\left(\Re\{\Phi_{i,\,\mathrm{E}}(cs_k)\,e^{-ycs_k}\} + \xi_k\Im\{\Phi_{i,\,\mathrm{E}}(cs_k)\,e^{-ycs_k}\}\right), \tag{28}$$

where $s_k \triangleq 1 + j\xi_k$, $\xi_k \triangleq \tan([2k-1]\pi/[2K])$, and K is a sufficiently large integer. According to [14] the best choice for c is that real–valued s which minimizes $\Phi_{i,\,\mathrm{E}}(s)\,e^{-ys}$. Since the minimum of $\Phi_{i,\,\mathrm{E}}(s)\,e^{-ys}$ is difficult to compute, we use $c = s_{\min} = y/\sigma_i^2$ instead, where $s_{\min}$ minimizes $\Phi_{i,\,\mathrm{GA}}(s)\,e^{-ys}$. We found that this choice guarantees fast convergence of the sum in Eq. (28) and $K = 200$ is sufficient to obtain accurate results. We note that although the evaluation of Eq. (28) requires the numerical integration of three integrals [Eqs. (13), (21)], the computation of $\mathrm{APD}_{\mathrm{E}}(y)$ is quite fast, since all integrals have finite limits.

4 BER of BPSK NB Signals

In this section, the BER of BPSK NB signals impaired by AWGN and MB–OFDM UWB interference is derived for transmission over non–fading and fading channels, respectively.

4.1 Preliminaries

In this subsection, we establish some basic results that are helpful for BER calculation. First, it is convenient to introduce the MGF $\Phi_{i+n,\,\mathrm{X}}(s)$, $\mathrm{X} \in \{\mathrm{E},\,\mathrm{GA},\,\mathrm{IGA}\}$, of the sum of MB–OFDM UWB interference and AWGN for the different interference models discussed in Section 3. Exploiting the fact that $i[k]$ and $n[k]$ are statistically independent $\Phi_{i+n,\,\mathrm{X}}(s)$ can be obtained as

$$\Phi_{i+n,\,\mathrm{X}}(s) = \Phi_{i,\,\mathrm{X}}(s)\,\Phi_n(s), \qquad \mathrm{X} \in \{\mathrm{E},\,\mathrm{GA},\,\mathrm{IGA}\}, \tag{29}$$

where $\Phi_n(s) = e^{s^2\sigma_n^2/2}$ denotes the MGF of $n[k]$. Using Eqs. (22), (23), and (29) it is not difficult to show that for a given NB channel gain a and BPSK signaling the GA and the IGA result in BERs

$$P_{e,\,\mathrm{GA}}(a) = Q\left(\sqrt{\frac{a^2}{\sigma_n^2+\sigma_i^2}}\right) \tag{30}$$

and

$$P_{e,\,\mathrm{IGA}}(a) = (1-\rho)\,Q\left(\sqrt{\frac{a^2}{\sigma_n^2}}\right) + \rho\,Q\left(\sqrt{\frac{a^2}{\sigma_n^2+\sigma_i^2/\rho}}\right), \tag{31}$$

respectively. On the other hand, for any of the considered interference models and a given NB channel amplitude a, we may express the BER of the BPSK NB receiver as

$$P_{e,\,\mathrm{X}}(a) = \int_{-\infty}^{-a} p_{i+n,\,\mathrm{X}}(x)\,\mathrm{d}x = \frac{1}{2\pi j}\int_{c-j\infty}^{c+j\infty} \Phi_{i+n,\,\mathrm{X}}(s)\,e^{-as}\,\frac{\mathrm{d}\,s}{s}, \qquad \mathrm{X} \in \{\mathrm{E},\,\mathrm{GA},\,\mathrm{IGA}\}, \tag{32}$$

where we have used as a similar approach as for derivation of Eq. (27). In the following subsections, we use Eqs. (30)–(32) for calculation of the BER for non–fading and fading channels.

4.2 BER in Non–Fading Channel

In this case, we may set $a = 1$ in Eqs. (30)–(32) and replace $P_{e,\,\mathrm{X}}(a)$ by $P_{e,\,\mathrm{X}}$. Using the definitions of the SNR and the SIR in Eq. (9), the GA and the IGA result in a BER of

$$P_{e,\,\mathrm{GA}} = Q\left(\sqrt{\frac{2}{\mathrm{SNR}^{-1}+\mathrm{SIR}^{-1}}}\right) \tag{33}$$

and

$$P_{e,\,\mathrm{IGA}} = (1-\rho)\,Q\left(\sqrt{2\mathrm{SNR}}\right) + \rho\,Q\left(\sqrt{\frac{2}{\mathrm{SNR}^{-1}+(\rho\,\mathrm{SIR})^{-1}}}\right), \tag{34}$$

respectively. For $\mathrm{SIR} \to \infty$, Eqs. (33) and (34) simplify to the well–known BER expression for BPSK transmission over a pure AWGN channel as expected, cf. [12, Eq. (5.2-5)]. We note that Eq. (34) can also be found in [7, 8] and is reported here only for completeness.

For the exact MB–OFDM UWB interference model a closed–form solution for $P_{e,\,\mathrm{E}}$ cannot be derived and the exact BER has to be evaluated numerically. This can be done efficiently by applying the Gauss–Chebyshev quadrature rule already used for derivation of Eq. (28). This yields

$$P_{e,\,\mathrm{E}} \simeq \frac{1}{K}\sum_{k=1}^{K/2}\left(\Re\{\Phi_{i+n,\,\mathrm{E}}(cs_k)\,e^{-cs_k}\} + \xi_k\Im\{\Phi_{i+n,\,\mathrm{E}}(cs_k)\,e^{-cs_k}\}\right), \tag{35}$$

where s_k, ξ_k, K, and c are defined after Eq. (28). A good choice for c guaranteeing fast convergence of the sum in Eq. (35) is $c = s_{\min} = 1/(\sigma_n^2+\sigma_i^2)$, where $s_{\min}$ minimizes $\Phi_{i+n,\,\mathrm{GA}}(s)\,e^{-s}$.

4.3 BER in General Fading Channels

For fading channels the NB amplitude a is a random variable with pdf $p_a(a)$. Furthermore, we introduce the pdf $p_\gamma(\gamma)$ of the squared amplitude $\gamma = a^2$. The average BER in fading channels can be obtained by averaging the expressions for $P_{e,\,\mathrm{X}}(a)$, $\mathrm{X} \in \{\mathrm{E},\ \mathrm{GA},\ \mathrm{IGA}\}$, given in Eqs. (30)–(32) over either $p_a(a)$ or $p_\gamma(\gamma)$.

For example, exploiting the alternative representation of the Q–function $Q(x) = \frac{1}{\pi}\int_0^{\pi/2}\exp(-\frac{x^2}{2\sin^2\varphi})\,\mathrm{d}\varphi$ [16] when averaging Eqs. (30) and (31) over $p_\gamma(\gamma)$ yields

$$P_{e,\,\mathrm{GA}} = \frac{1}{\pi}\int_0^{\pi/2}\Phi_\gamma\left(\frac{1}{(\mathrm{SNR}^{-1}+\mathrm{SIR}^{-1})\sin^2\varphi}\right)\mathrm{d}\varphi \tag{36}$$

and

$$P_{e,\,\mathrm{IGA}} = \frac{1-\rho}{\pi}\int_0^{\pi/2}\Phi_\gamma\left(\frac{\mathrm{SNR}}{\sin^2\varphi}\right)\mathrm{d}\varphi + \frac{\rho}{\pi}\int_0^{\pi/2}\Phi_\gamma\left(\frac{1}{(\mathrm{SNR}^{-1}+(\rho\mathrm{SIR})^{-1})\sin^2\varphi}\right)\mathrm{d}\varphi, \tag{37}$$

respectively. Here, $\Phi_\gamma(s) \triangleq \mathcal{E}\{e^{-\gamma s}\}$ denotes the MGF (as defined here) of γ. For the most important fading distributions (Rayleigh, Ricean, Nakagami–m, Nakagami–q) closed–form expressions for $\Phi_\gamma(s)$ can be easily obtained, cf. e.g. [16, Table 3]. For example, for Rayleigh and Nakagami–m

fading $\Phi_\gamma(s) = 1/(1+s)$ and $\Phi_\gamma(s) = 1/(1+s/m)^m$ result, respectively. Using Eqs. (36) and (37) the BER for the GA and the IGA can be efficiently computed by numerically evaluating one–dimensional integrals with finite limits. We note that for Rayleigh fading Eqs. (36) and (37) can be further simplified and closed–form expressions for $P_{e,\,\mathrm{GA}}$ and $P_{e,\,\mathrm{IGA}}$ can be obtained, cf. Section 4.4. This is also possible for Nakagami–m fading by exploiting results in [17].

On the other hand, averaging Eq. (32) over $p_a(a)$, we obtain for both the exact and the approximate interference models

$$P_{e,\,\mathrm{X}} = \mathcal{E}\{P_{e,\,\mathrm{X}}(a)\} = \frac{1}{2\pi j}\int_{c-j\infty}^{c+j\infty} \Phi_{i+n,\,\mathrm{X}}(s)\,\Phi_a(s)\,\frac{\mathrm{d}\,s}{s}, \qquad \mathrm{X} \in \{\mathrm{E},\,\mathrm{GA},\,\mathrm{IGA}\}, \tag{38}$$

where $\Phi_a(s) \triangleq \mathcal{E}\{e^{-as}\}$ denotes the MGF of a. Applying again a Gauss–Chebyshev quadrature rule, we obtain

$$P_{e,\,\mathrm{X}} \simeq \frac{1}{K}\sum_{k=1}^{K/2} \left(\Re\{\Phi_{i+n,\,\mathrm{X}}(cs_k)\,\Phi_a(cs_k)\} + \xi_k \Im\{\Phi_{i+n,\,\mathrm{X}}(cs_k)\,\Phi_a(cs_k)\}\right), \tag{39}$$

where $\mathrm{X} \in \{\mathrm{E},\,\mathrm{GA},\,\mathrm{IGA}\}$ and s_k, ξ_k, K, and c have been defined before. The amplitude MGF $\Phi_a(s)$ is readily available in the literature for all relevant fading distributions. For example, the MGFs $\Phi_a(s)$ for Rayleigh, Ricean, Nakagami–q, and Nakagami–m fading can be found in [18, Table I][7]. Consequently, Eq. (39) can be used for efficient numerical computation of both the exact and the approximate BERs for any relevant fading distribution. For fading channels it is more difficult to find good values for c than for non–fading channels since $\Phi_a(s)$ typically involves confluent hypergeometric series, cf. [18, Table I]. A suitable value is $c = \Re\{s'\}/2$, where s' denotes that zero of $\Phi_a(s)$ which has minimum real part. s' can be found using standard numerical procedures [19]. Note that for the GA and the IGA Eq. (39) is an alternative to Eqs. (36) and (37), respectively, where both options entail approximately the same complexity.

4.4 BER in Rayleigh Fading

For Rayleigh fading Eqs. (36) and (37) can be further simplified to

$$P_{e,\,\mathrm{GA}} = \frac{1}{2}\left(1 - \frac{1}{\sqrt{1+\mathrm{SNR}^{-1}+\mathrm{SIR}^{-1}}}\right) \tag{40}$$

[7] Strictly speaking the characteristic function $\Phi_a(-j\omega)$ is given in [18, Table I]. However, the MGF can be easily obtained by applying the substitution $\omega = js$.

and

$$P_{e,\mathrm{IGA}} = \frac{1}{2}\left(1 - \frac{1-\rho}{\sqrt{1+\mathrm{SNR}^{-1}}} - \frac{\rho}{\sqrt{1+\mathrm{SNR}^{-1}+(\rho\mathrm{SIR})^{-1}}}\right), \tag{41}$$

respectively. For $\mathrm{SIR} \to \infty$ both Eq. (40) and Eq. (41) simplify to the well–known BER expression for BPSK transmission over a Rayleigh fading channel impaired by AWGN, cf. [12, Eq. (14.3.7)]. Furthermore, it can be shown that for $\mathrm{SNR} \gg 1$ and $\mathrm{SIR} \gg 1$ the GA, the IGA, and the exact MB–OFDM UWB interference model all lead to the same BER

$$P_{e,\mathrm{X}} \simeq \frac{1}{4}\left(\mathrm{SNR}^{-1} + \mathrm{SIR}^{-1}\right), \qquad \mathrm{X} \in \{\mathrm{E},\, \mathrm{GA},\, \mathrm{IGA}\}. \tag{42}$$

For the GA and the IGA Eq. (42) can be proved by applying $1/\sqrt{1+x} \simeq 1 - x/2$, $|x| \ll 1$, in Eqs. (40) and (41), whereas the exact case is discussed in Appendix B.

Eq. (42) shows that for high SNRs and high SIRs the exact BER $P_{e,\mathrm{E}}$ in Rayleigh fading only depends on the SNR and the SIR but is independent of other system parameters such as B_s, Δf, and f_0.

5 Results and Discussions

In this section, we use our analytical methods presented in the previous sections to study the performance of BPSK NB receivers impaired by MB–OFDM UWB interference, AWGN, and possibly fading. The MB–OFDM UWB parameters given in Table 1, an SRRC NB pulse with roll–off $r = 0.35$, and the channel model introduced in Section 2 are employed unless stated otherwise. In addition, to avoid distortion of the results by the null sub–carriers, we set $f_0 = 10\Delta f$ unless specified otherwise.

5.1 APD Plot

Fig. 2 shows APD plots for MB–OFDM UWB interference with $\sigma_i^2 = 1$, $f_0 = 10\Delta f$, and $N_B = 3$. The curves in Fig. 2 were generated using the results in Section 3.3 and adopting the format recommended by the NTIA in [11, Appendix D], i.e., the x–axis shows the percentage of time for which $|i[k]|$ exceeds the ordinate. The GA yields approximately a straight line and is approached by the exact APD for small (normalized) NB signal bandwidths $B_s/\Delta f$, whereas the IGA is approached for large $B_s/\Delta f$, cf. Section 3.2. The more often a given ordinate is exceeded on average (i.e.,

the larger the corresponding x–axis value), the higher the corresponding bit error rate will be. For communications applications the x–axis interval below 1% is most relevant as it reflects the behavior of the tails of the corresponding pdf. Therefore, Fig. 2 shows that for certain NB signal bandwidths MB–OFDM UWB interference is more favorable than Gaussian noise with equal variance, whereas impulsive noise has a more detrimental effect in the interval of interest. For example, $|i[k]|$ exceeds $20\log_{10}(y) = 6$ dB for $B_s/\Delta f = 0.15$ only 10^{-4} % of the time, while Gaussian noise and impulsive noise exceed this level 0.5% and 4% of the time, respectively. The APDs in Fig. 2 suggest that the impact of MB–OFDM UWB interference on a NB receiver strongly depends on the bandwidth of the NB signal.

5.2 BER in Non–Fading Channel

In Fig. 3, we investigate the dependence of the exact BER on the NB pulse shape as a function of $B_s/\Delta f$. SRRC impulses with various roll–off factors r are compared with a REC pulse of duration $T_s = 1/B_s$ for $10\log_{10}(\mathrm{SNR}) = 10$ dB, $f_0 = 10\Delta f$, $N_B = 3$, and various SIRs. As expected, all exact BERs approach the respective GAs and the IGAs for very small and very large NB signal bandwidths, respectively. The GA is faster approached for smaller r than for larger r since in the former case the corresponding time domain pulse shape decays more slowly. For medium NB bandwidths ($0.05 \leq B_s/\Delta f \leq 5$) the exact BER depends significantly on the NB pulse shape, especially for low SIRs. The simulation results for $r = 0.2$ and $r = 0.8$ confirm the exact BER analysis.

The effect of the frequency offset f_0 between the NB signal and the MB–OFDM signal on the exact BER is studied in Figs. 4 and 5. Fig. 4 shows the exact BER vs. $f_0/\Delta f$ for the interference limited case (i.e., $\mathrm{SNR} \to \infty$) assuming $B_s = \Delta f$ and $N_B = 3$. Numerical results (solid lines) and simulation results (markers) are in excellent agreement. For $10\log_{10}(\mathrm{SIR}) > 6$ dB the BER strongly depends on f_0, where values of f_0 close to the sub–carrier center frequency of $10\Delta f$ result in a lower BER. We note that as long as border effects can be neglected the BER is periodic in f_0 with period Δf. Fig. 5 depicts BER vs. $B_s/\Delta f$ for $10\log_{10}(\mathrm{SNR}) = 10$ dB, $N_B = 3$, various $f_0/\Delta f$, and various SIRs. The exact BER approaches the GA faster if the NB carrier frequency is between two MB–OFDM sub–carriers (e.g. $f_0/\Delta f = 10.5$), and it becomes independent of f_0 if the NB signal bandwidth exceeds twice the MB–OFDM sub–carrier spacing ($B_s > 2\Delta f$).

In Fig. 6, we investigate the impact of N_B on the exact BER for $10\log_{10}(\mathrm{SNR}) = 10$ dB,

$10\log_{10}(\mathrm{SIR}) = 15$ dB, and $f_0 = 10\Delta f$. While the exact BER for large B_s and the IGA depend on N_B, the exact BER for small B_s and the GA are independent of N_B. However, the exact BER approaches the GA faster for small N_B as expected, cf. Section 3.2. The difference between GA and IGA increases with increasing N_B, as in the latter case the interference becomes more impulsive for larger N_B. We note that even for $N_B = 1$ (i.e., conventional OFDM with only one band) GA and IGA are not identical because of the non–zero prefix duration T_P and the non–zero guard interval T_G, which are responsible for $\rho = 1/(\Delta f T_i) < 1$ in this case.

Figs. 3, 5, and 6 show that for a given SIR NB signals with small bandwidths B_s are less affected by MB–OFDM UWB interference than NB signals with large B_s. In addition, for non–fading channels with the considered parameters the IGA upper–bounds the exact BER, whereas the GA is approached from below by the exact BER for small NB signal bandwidths. In fact, from the comparison of the GA and the exact BER in Figs. 3, 5, and 6 we can also conclude that in non–fading channels for low–to–medium values of B_s the pdf of MB–OFDM UWB interference has a more favorable impact on error performance than the Gaussian pdf, cf. discussion in Section 5.1. We note that our analysis is restricted to uncoded NB systems and it is difficult to draw conclusions for coded NB systems from it. For example, it is well–known that the capacity of channels with impulsive noise is higher than that of channels with Gaussian noise [20]. The analysis of coded NB systems under MB–OFDM interference is an interesting topic for future research.

5.3 BER in Fading Channel

Fig. 7 illustrates the dependence of the exact BER on the NB signal bandwidth B_s for Nakagami–m fading with $10\log_{10}(\mathrm{SNR}) = 10$ dB, $10\log_{10}(\mathrm{SIR}) = 10$ dB, $f_0 = 10\Delta f$, and $N_B = 3$. We note that $m = 1$ and $m \to \infty$ correspond to Rayleigh fading and no fading, respectively. It is interesting to observe that the performance difference between GA and IGA increases with increasing m. Similarly, while the exact BER is almost independent of B_s for $m = 0.5,\ 1,\ 2$ (cf. also Section 4.4), a strong dependence of the exact BER on B_s can be observed for $m \geq 5$. This clearly shows that MB–OFDM UWB interference should not be analyzed in isolation (as is done with the APD plots advocated by the NTIA), but only in connection with the underlying NB channel.

5.4 Impact of Different UWB Channel Models

So far we have assumed a flat channel model. While this is an appropriate model for small NB signal bandwidths B_s, a frequency–selective channel model may be more appropriate for large B_s. Therefore, we compare in Fig. 8 the analytical BER obtained for the channel model described in Section 2 with simulation results for one (typical) realization of the CM1 and CM4 UWB channel models defined in [21]. We have assumed a flat and non–fading NB channel for all BER curves shown in Fig. 8, i.e., we assume that only the MB–OFDM interference channel is frequency selective. For CM1 and CM4 the impulse response is multiplied by a log–normal shadowing term, cf. [21]. To separate the effects of frequency–selectivity and log–normal shadowing, we show in Fig. 8 simulation results obtained with and without the log–normal term. Fig. 8 shows that the exact BER obtained for a flat interference channel can serve as a good estimate for the BER for CM1 and CM4 UWB interference channels. The log–normal shadowing causes the simulated BER to deviate from the exact BER also for small NB signal bandwidths, since the averaging of individual interference terms which is essential for application of the central limit theorem does not affect the log–normal shadowing. For large NB signal bandwidths and no shadowing the deviation from the exact BER is larger for the more severely frequency–selective CM4 channel than for the CM1 channel. However, for CM4 and large B_s the effects of shadowing and frequency–selectivity seem to balance each other and the simulated BER is very close to the exact BER.

6 Conclusions

In this paper, we have provided a comprehensive analysis of MB–OFDM UWB interference and its impact on BPSK NB receivers. Based on the MGF of MB–OFDM UWB interference, efficient methods for numerical evaluation of the exact interference APD and the exact BER of a BPSK NB receiver have been developed. Furthermore, we have introduced a GA and an IGA for MB–OFDM UWB interference which result in simpler APD and BER expressions than the exact interference model. Our numerical results suggest that, in general, the GA and the IGA give accurate results for $B_s < 0.05\Delta f$ and $B_s > 5\Delta f$, respectively. For the special case of a Rayleigh fading NB channel both approximations are tight for sufficiently high SNR and SIR regardless of B_s. However, for $0.05\Delta f \leq B_s \leq 5\Delta f$, in general, the BER of the NB receiver strongly depends on the carrier frequency offset f_0 between the NB signal and the MB–OFDM signal, the NB signal bandwidth,

the number of MB–OFDM frequency bands, and the NB pulse shape.

A Periodicity of $\Phi_{i|\tau_k}(s,\,\tau_k)$

The periodicity of $\Phi_{i|\tau_k}(s,\,\tau_k)$ can be proved by replacing τ_k by $\tau_k' \triangleq \tau_k + N_B\lambda T_i$ in Eq. (20)

$$\begin{aligned}
\Phi_{i|\tau_k}(s,\,\tau_k') &= \frac{1}{2\pi}\int_{2\pi}\prod_{\kappa=-\infty}^{\infty}\prod_{\substack{n=-N_s/2\\ n\neq 0}}^{N_s/2}\cosh(s\,\Re\{g e^{j\theta}e^{j2\pi f_0 N_B\kappa T_i}\beta_n(\tau_k + N_B\lambda T_i - N_B\kappa T_i)\})\\
&\qquad \cosh\left(s\,\Im\{g e^{j\theta}e^{j2\pi f_0 N_B\kappa T_i}\beta_n(\tau_k + N_B\lambda T_i - N_B\kappa T_i)\}\right)\,\mathrm{d}\theta,\\
&= \frac{1}{2\pi}\int_{2\pi}\prod_{\kappa'=-\infty}^{\infty}\prod_{\substack{n=-N_s/2\\ n\neq 0}}^{N_s/2}\cosh(s\,\Re\{g e^{j\theta}e^{j2\pi f_0 N_B(\kappa'+\lambda)T_i}\beta_n(\tau_k - N_B\kappa' T_i)\})\\
&\qquad \cosh\left(s\,\Im\{g e^{j\theta}e^{j2\pi f_0 N_B(\kappa'+\lambda)T_i}\beta_n(\tau_k - N_B\kappa' T_i)\}\right)\,\mathrm{d}\theta\\
&= \frac{1}{2\pi}\int_{2\pi}\prod_{\kappa'=-\infty}^{\infty}\prod_{\substack{n=-N_s/2\\ n\neq 0}}^{N_s/2}\cosh(s\,\Re\{g e^{j\theta'}e^{j2\pi f_0 N_B\kappa' T_i}\beta_n(\tau_k - N_B\kappa' T_i)\})\\
&\qquad \cosh\left(s\,\Im\{g e^{j\theta'}e^{j2\pi f_0 N_B\kappa' T_i}\beta_n(\tau_k - N_B\kappa' T_i)\}\right)\,\mathrm{d}\theta'\\
&= \Phi_{i|\tau_k}(s,\,\tau_k), \qquad (43)
\end{aligned}$$

where we have used the substitutions $\kappa' = \kappa - \lambda$ and $\theta' = \theta + 2\pi f_0 N_B\lambda T_i$, respectively.

B Asymptotic BER in Rayleigh Fading

Based on Eq. (6) we can express the exact BER as

$$\begin{aligned}
P_{e,\mathrm{E}} &= \Pr\{|a_c b[k] + i_c[k] + n_c[k] - a_c b[k]|^2 > |a_c b[k] + i_c[k] + n_c[k] + a_c b[k]|^2\}\\
&= \Pr\{|a_c|^2 + a_c(i_c[k] + n_c[k])^*/2 + a_c^*(i_c[k] + n_c[k])/2 < 0\}. \qquad (44)
\end{aligned}$$

For Rayleigh fading a_c is a zero–mean Gaussian random variable. Using the results of [12, Appendix B] we can express the exact BER conditioned on $i_c[k]$ as

$$P_{e|i_c,\,\mathrm{E}} = \frac{1}{2}\left(1 - \frac{I_0(y^2)e^{-y^2}}{\sqrt{1+2\sigma_n^2}}\right), \qquad (45)$$

where $y^2 \triangleq |i_c[k]|^2/(2\sqrt{1+2\sigma_n^2})$ and $I_0(\cdot)$ denotes the zeroth order Bessel function of the first kind. Assuming $|i_c[k]|^2 \ll 1$ and $\sigma_n^2 \ll 1$ and using the relations $1/\sqrt{1+x} \simeq 1 - x/2$, $I_0(x) \simeq 1 - x^2/4$, and $e^{-x} \simeq 1 - x$, which are all valid for $x \ll 1$, we obtain from Eq. (45)

$$P_{e|i_c,\mathrm{E}} = \sigma_n^2/2 + |i_c[k]|^2/4. \tag{46}$$

Averaging Eq. (46) over the (unknown) pdf of the interference yields the (unconditional) BER

$$P_{e,\mathrm{E}} = \sigma_n^2/2 + \sigma_i^2/2, \tag{47}$$

where we have used $\mathcal{E}\{|i_c[k]|^2\} = 2\sigma_i^2$ which follows from the fact that $i_c[k]$ is rotationally symmetric since θ_g is uniformly distributed in $[-\pi, \pi)$. Now, Eq. (42) is easily obtained by combining Eq. (47) with Eq. (9).

References

[1] A. Swami, B. Sadler, and J. Turner. On the Coexistence of Ultra-Wideband and Narrowband Radio Systems. In *Proceedings of IEEE Military Communications Conference*, pages 16–19, Washington, October 2001.

[2] J.R. Foerster. Interference Modeling of Pulse-based UWB Waveforms on Narrowband Systems. In *Proceedings of IEEE Vehicular Technology Conference (VTC)*, pages 1931–1935, Birmingham, Al., May 2002.

[3] Z. Ye, A.S. Madhukumar, and F. Chin. Power Spectral Density and In-Band Interference Power of UWB Signals at Narrowband Systems. In *Proceedings of the International Conference on Communications (ICC)*, pages 3561–3565, Paris, June 2004.

[4] R. Giuliano and F. Mazzenga. On the Coexistence of Power Controlled Ultrawide-Band Systems with UMTS, GPS, DCS1800, and Fixed Wireless Systems. *IEEE Trans. Veh. Technol.*, VT-54:62–81, January 2005.

[5] IEEE P802.15. Multiband OFDM Physical Layer Proposal for IEEE 802.15 Task Group 3a (Doc. Number P802.15-03/268r3). March 2004.

[6] ECMA. Standard ECMA-368: High Rate Ultra Wideband PHY and MAC Standard. *[Online] http://www.ecma-international.org/publications/standards/Ecma-368.htm*, December 2005.

[7] MultiBand OFDM Alliance SIG. In-band Interference Properties of MB–OFDM. *[Online] http://www.multibandofdm.org/papers/MBOA-SIG-2004-in-band-interference-properties-mb-ofdm.ppt*, September 2004.

[8] C.A. Corral and S. Emami and G. Rasor. Model of Multi-Band OFDM Interference on Broadband QPSK Receivers. In *Proceedings of the IEEE International Conference on Acoustics, Speech, and Signal Processing (ICASSP)*, pages 629–632, Philadelphia, November 2005.

[9] IEEE P802.15. Coexistence of Multi-band OFDM and IEEE 802.11a: Interference Measurements (Doc. Number P802.15-04/017r0). January 2004.

[10] IEEE P802.15. Impact of MB–OFDM and DS–UWB Interference – Part 2 (Doc. Number P802.15-05/0039r0). January 2005.

[11] National Telecommunications and Information Administration (NTIA). Interference Potential of Ultrawideband Signals (NTIA Report TR-05-419). *[Online] http://www.its.bldrdoc.gov/pub/ntia-rpt/05-419/05-419.pdf*, February 2005.

[12] J.G. Proakis. *Digital Communications*. McGraw–Hill, New York, forth edition, 2000.

[13] A.V. Oppenheim and A.S. Willsky. *Signals and Systems*. Prentice–Hall, Inc., Upper Saddle River, New Jersey, 1996.

[14] E. Biglieri, G. Caire, G. Taricco, and J. Ventura-Traveset. Computing Error Probabilities over Fading Channels: a Unified Approach. *European Transactions on Telecommunications*, 9:15–25, January-Feburary 1998.

[15] K. Cho and D. Yoon. On the General BER Expression of One- and Two-Dimensional Amplitude Modulations. *IEEE Trans. Commun.*, COM-50:1074–1080, July 2002.

[16] M.K. Simon and M.-S. Alouini. A Unified Analysis to the Performance Analysis of Digital Communication over Generalized Fading Channels. *Proceedings of the IEEE*, 86:1860–1877, September 1998.

[17] A. Annamalai and C. Tellambura. Error Rates for Nakagami-m Fading Multichannel Reception of Binary and M-ary Signals. *IEEE Trans. Commun.*, COM-49:58–68, January 2001.

[18] A. Annamalai, C. Tellambura, and V.K. Bhargava. A General Method for Calculating Error Probabilities Over Fading Channels. *IEEE Trans. Commun.*, COM-53:841–852, May 2005.

[19] T.K. Moon and W.C. Stirling. *Mathematical Methods and Algorithms for Signal Processing*. Prentice Hall, New York, 2000.

[20] D. Stopler and R. Zamir. Capacity and Error Probability in Single-Tone and Multitone Multiple Access over an Impulsive Channel. *IEEE Trans. Commun.*, COM-49:506–517, March 2001.

[21] A.F. Molisch, J.R. Foerster, and M. Pendergrass. Channel Models for Ultrawideband Personal Area Networks. *IEEE Wireless Communications*, 10:14–21, December 2003.

Tables and Figures:

Table 1: MB–OFDM parameters [5].

Number of non–null sub–carriers	$N_s = 122$
Sub–carrier spacing	$\Delta f = 4.125$ MHz
OFDM symbol duration	$T_i = 312.5$ ns
Prefix duration	$T_P = 60.61$ ns
Guard interval	$T_G = 9.47$ ns
Frequency bands	$N_B = 3$

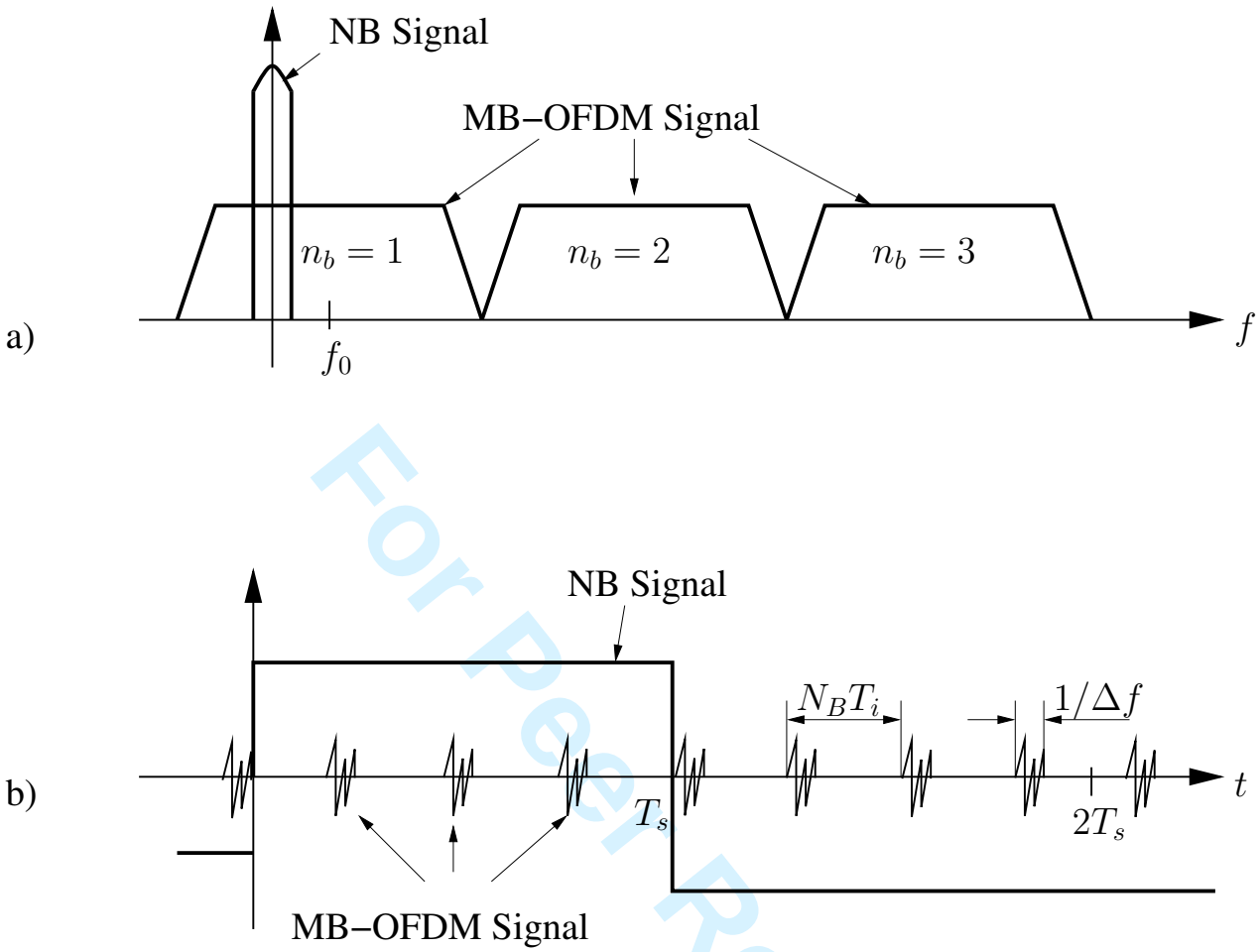

Figure 1: NB signal and MB–OFDM signal in a) frequency domain and b) time domain for $N_B = 3$. We note that for the time domain representation of the MB–OFDM signal only the contribution of the relevant first frequency band is depicted.

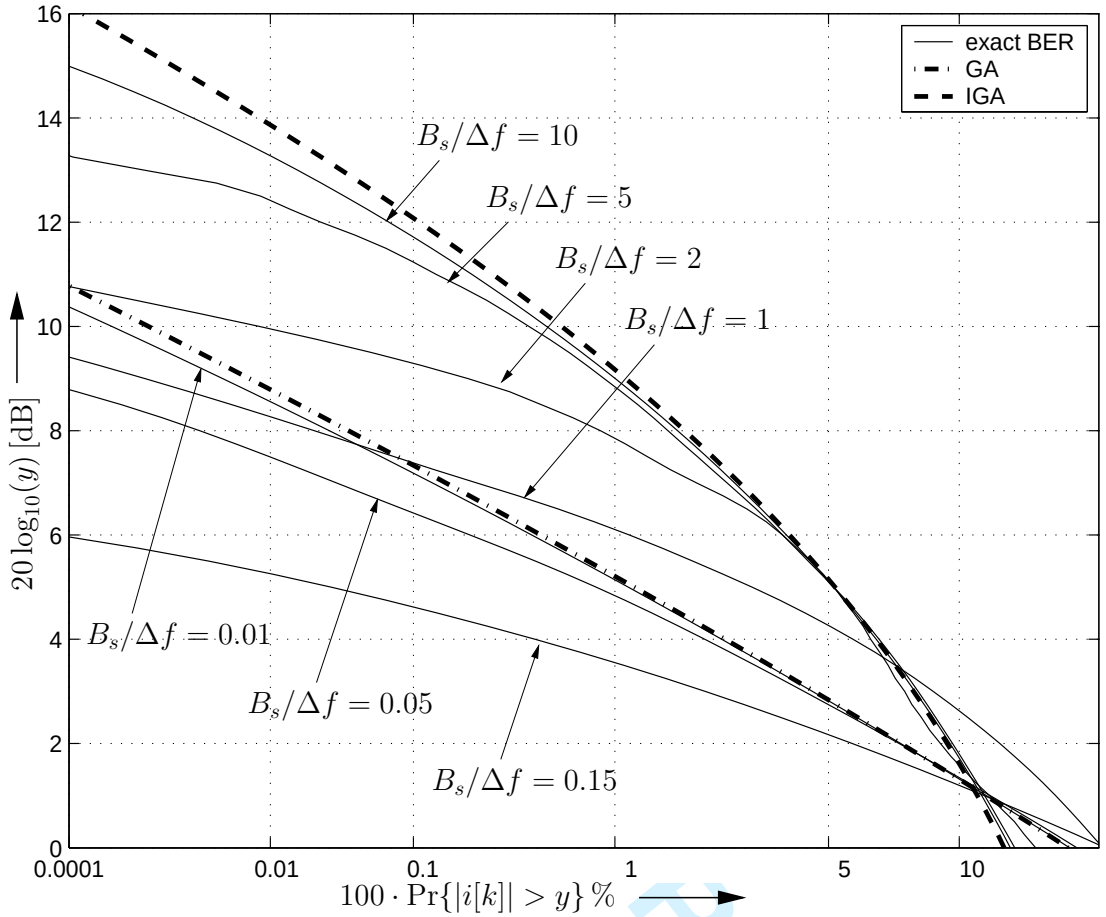

Figure 2: APD plot for different NB signal bandwidths $B_s/\Delta f$. $\sigma_i^2 = 1$, $f_0 = 10\Delta f$, and $N_B = 3$. Exact APD [Eq. (28)], GA [Eq. (25)], and IGA [Eq. (26)].

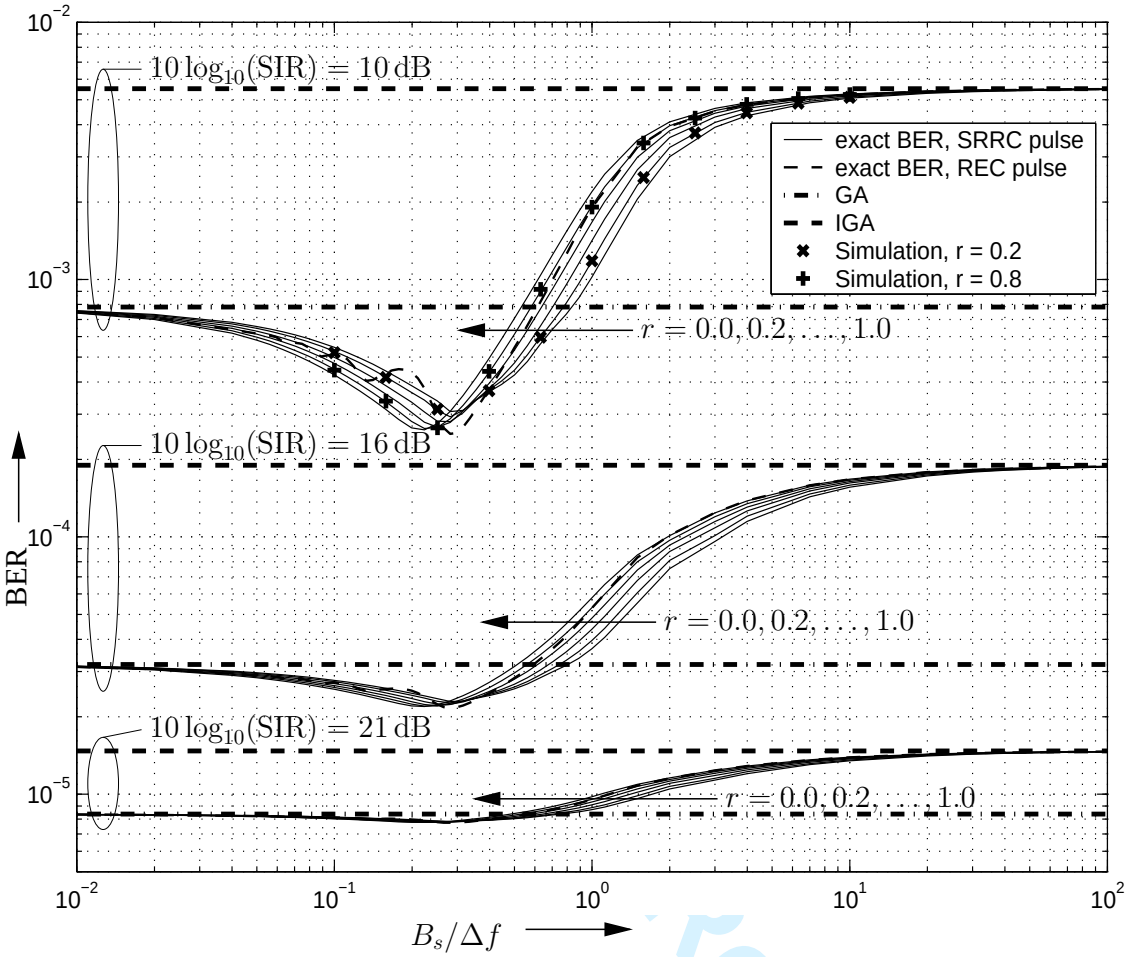

Figure 3: BER vs. $B_s/\Delta f$ for different NB pulse shapes and different SIRs. $10\log_{10}(\text{SNR}) = 10$ dB, $f_0 = 10\Delta f$, and $N_B = 3$. Exact BER [Eq. (35)], GA [Eq. (33)], and IGA [Eq. (34)]. Markers: Simulation results.

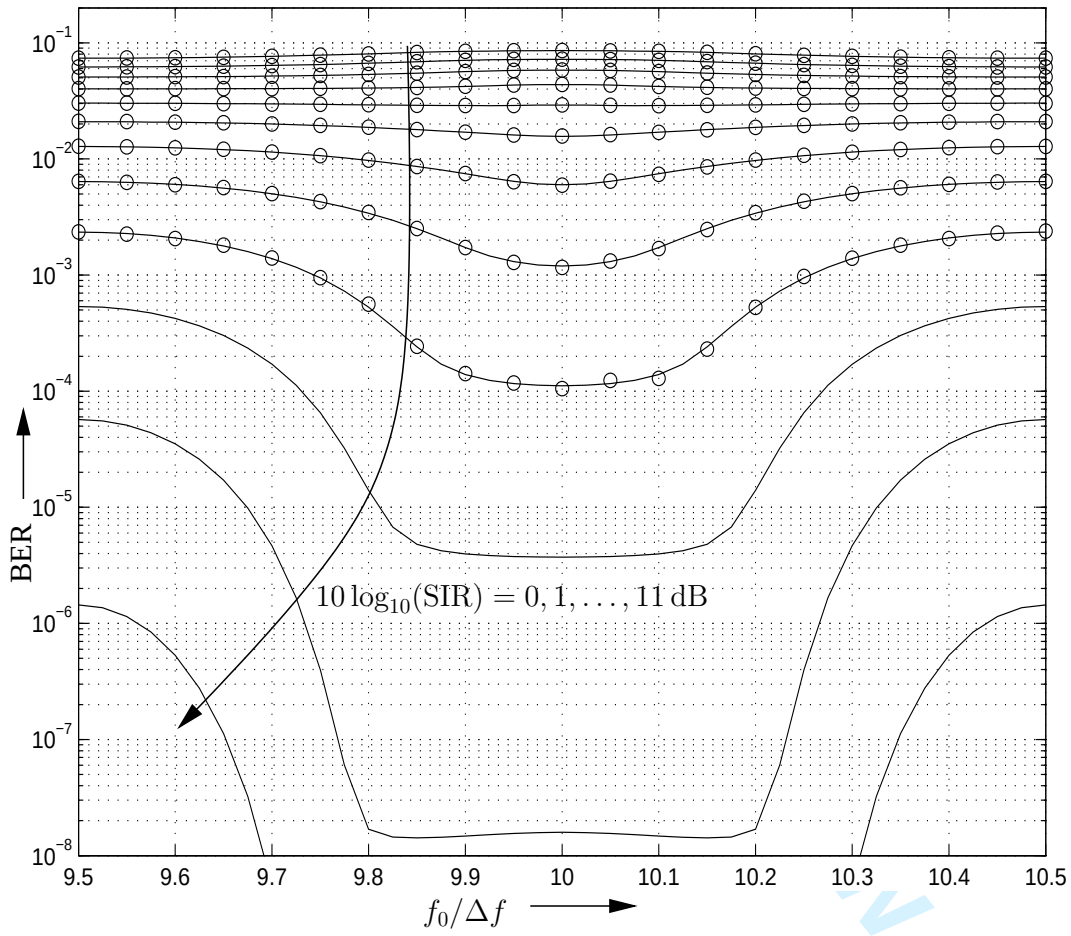

Figure 4: Exact BER vs. $f_0/\Delta f$ for different SIRs. Interference limited case (SNR $\to \infty$), $B_s = \Delta f$, and $N_B = 3$. Markers: Simulation results. Solid lines: Numerical results [Eq. (35)].

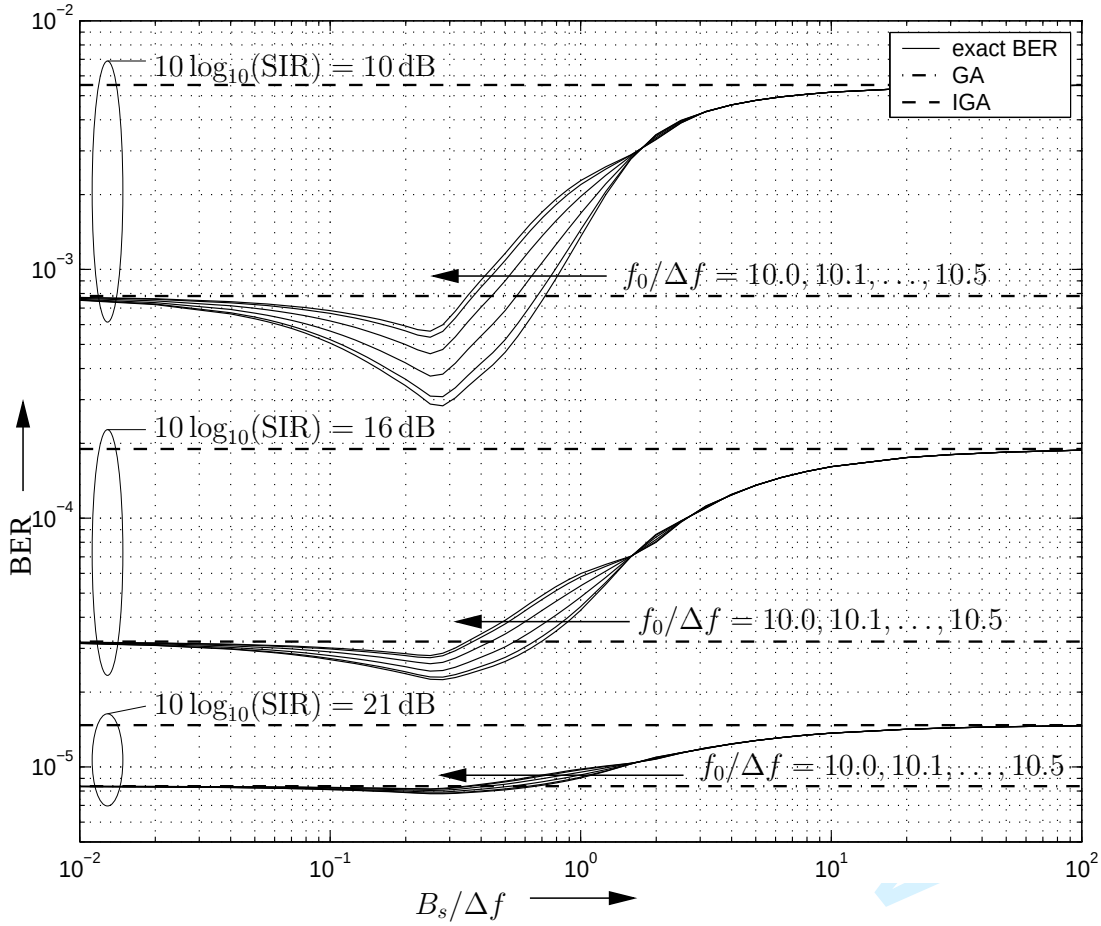

Figure 5: BER vs. $B_s/\Delta f$ for different $f_0/\Delta f$ and different SIRs. $10\log_{10}(\mathrm{SNR}) = 10$ dB and $N_B = 3$. Exact BER [Eq. (35)], GA [Eq. (33)], and IGA [Eq. (34)].

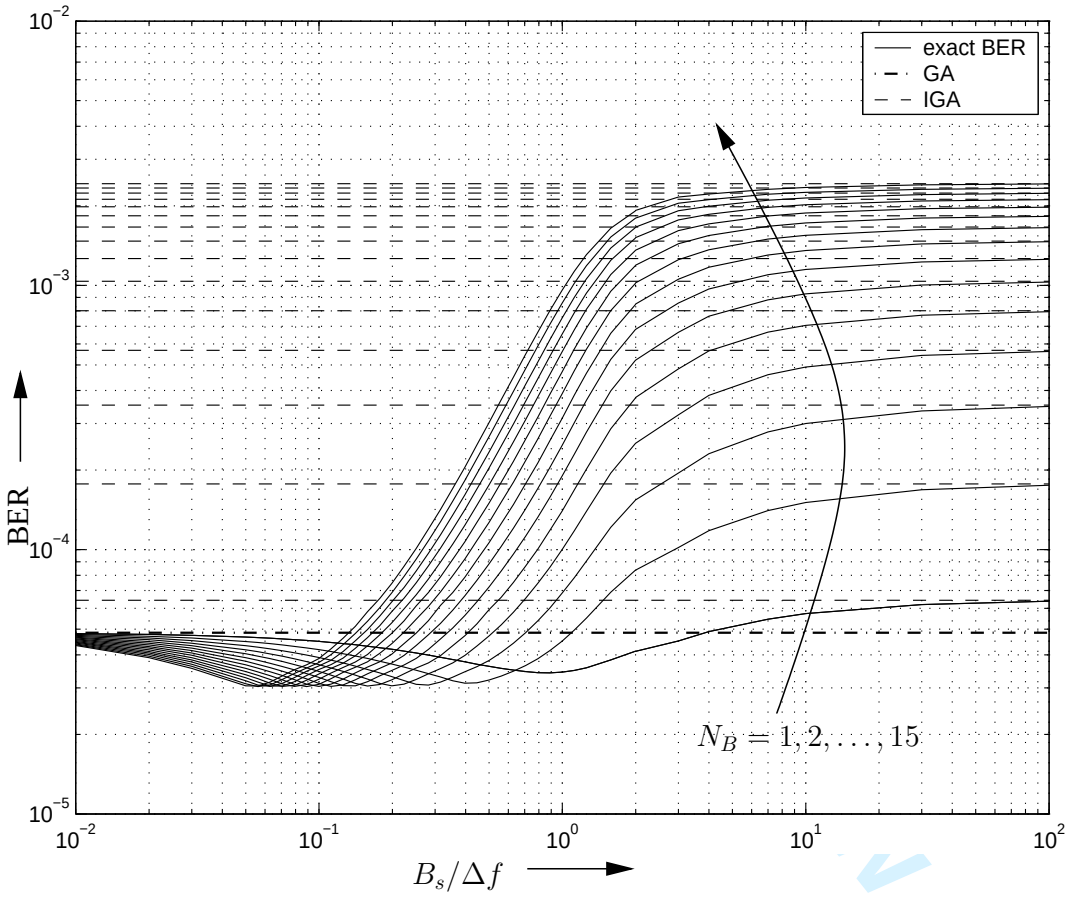

Figure 6: BER vs. $B_s/\Delta f$ for different N_B. $10\log_{10}(\text{SNR}) = 10$ dB, $10\log_{10}(\text{SIR}) = 15$ dB, and $f_0 = 10\Delta f$. Exact BER [Eq. (35)], GA [Eq. (33)], and IGA [Eq. (34)].

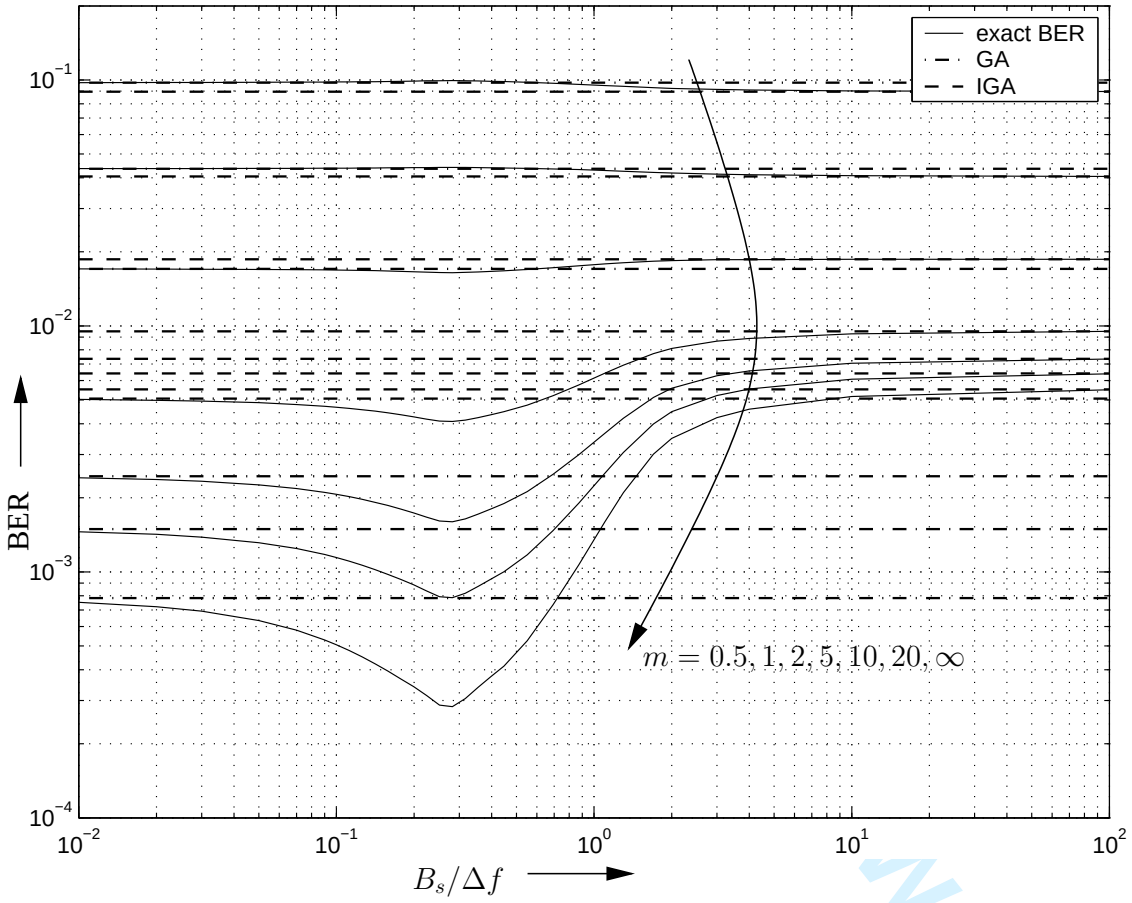

Figure 7: BER vs. $B_s/\Delta f$ for different fading parameters m. $10\log_{10}(\text{SNR}) = 10$ dB, $10\log_{10}(\text{SIR}) = 10$ dB, $f_0 = 10\Delta f$, and $N_B = 3$. Exact BER [Eq. (39)], GA [Eq. (36)], and IGA [Eq. (37)].

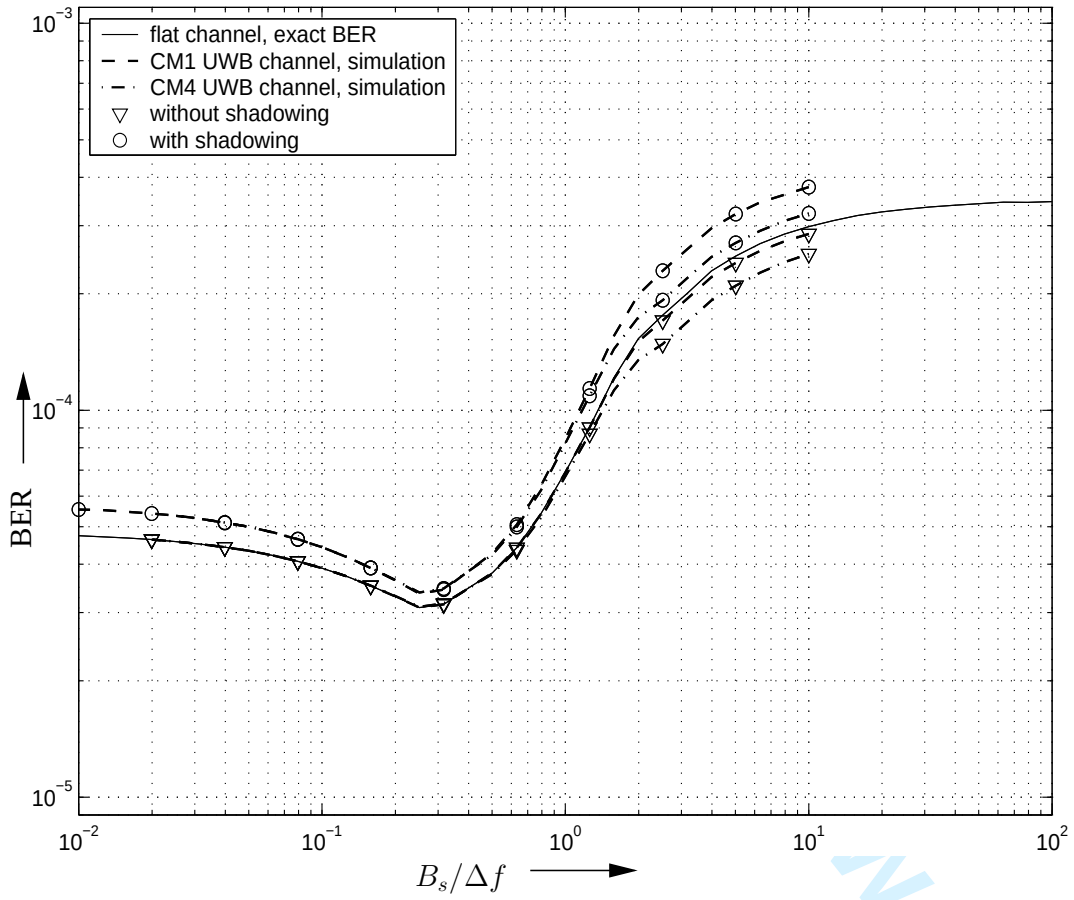

Figure 8: BER vs. $B_s/\Delta f$ for different interference channels. $10\log_{10}(\text{SNR}) = 10$ dB, $10\log_{10}(\text{SIR}) = 15$ dB, and $f_0 = 10\Delta f$. Exact BER for flat channel [Eq. (35)] and simulation results for one realization of CM1 and CM4 UWB channel models.